Glycosaminoglycans exhibit distinct interactions and signaling with BMP2 according to their nature and localization

Jean Le Pennec, Olga Makshakova, Paola Nevola, Farah Fouladkar, Evelyne Gout, Paul Machillot, Mélanie Friedel-Arboleas, Catherine Picart, Serge Perez, Andrea Vortkamp, et al.

Carbohydrate Polymers 341 (2024) 122294

Contents lists available at ScienceDirect

Carbohydrate Polymers

journal homepage: www.elsevier.com/locate/carbpol

Glycosaminoglycans exhibit distinct interactions and signaling with BMP2 according to their nature and localization

Jean Le Pennec [a], Olga Makshakova [b,c], Paola Nevola [a,d], Farah Fouladkar [a], Evelyne Gout [e], Paul Machillot [a], Mélanie Friedel-Arboleas [e], Catherine Picart [a], Serge Perez [f], Andrea Vortkamp [g], Romain R. Vivès [e,*], Elisa Migliorini [a,*]

[a] Univ. Grenoble Alpes, INSERM, CEA, CNRS, U1292 Biosanté, EMR 5000, Grenoble, France
[b] Faculty of Biology, University of Freiburg, 79104 Freiburg, Germany
[c] Signalling Research Centres BIOSS and CIBSS, Synthetic Biology of Signalling Processes Lab, University of Freiburg, 79104 Freiburg, Germany
[d] Dipartimento di Ingegneria Chimica dei Materiali e della Produzione Industriale, University of Naples Federico II, Napoli, Italy
[e] Univ. Grenoble Alpes, CNRS, CEA, IBS, Grenoble, France
[f] Univ. Grenoble Alpes, CNRS, Centre de Recherche sur les Macromolécules Végétales, Grenoble, France
[g] Developmental Biology, Centre for Medical Biotechnology, University Duisburg-Essen, Essen, Germany

ARTICLE INFO

Keywords:
Glycosaminoglycans
Bone morphogenetic protein 2
Binding affinity
Heparan sulfate sulfation pattern
Biomaterials
Extracellular matrix

ABSTRACT

The role of glycosaminoglycans (GAGs) in modulating bone morphogenetic protein (BMP) signaling represents a recent and underexplored area. Conflicting reports suggest a dual effect: some indicate a positive influence, while others demonstrate a negative impact. This duality suggests that the localization of GAGs (either at the cell surface or within the extracellular matrix) or the specific type of GAG may dictate their signaling role. The precise sulfation patterns of heparan sulfate (HS) responsible for BMP2 binding remain elusive. BMP2 exhibits a preference for binding to HS over other GAGs. Using well-characterized biomaterials mimicking the extracellular matrix, our research reveals that HS promotes BMP2 signaling in the extracellular space, contrary to chondroitin sulfate (CS), which enhances BMP2 bioactivity at the cell surface. Further observations indicate that a central IdoA (2*S*)-GlcNS (6S) tri-sulfated motif within HS hexasaccharides enhances binding. Nevertheless, BMP2 exhibits a degree of adaptability to various HS sulfation types and sequences. Molecular dynamic simulations attribute this adaptability to the BMP2 N-terminal end flexibility. Our findings illustrate the complex interplay between GAGs and BMP signaling, highlighting the importance of localization and specific sulfation patterns. This understanding has implications for the development of biomaterials with tailored properties for therapeutic applications targeting BMP signaling pathways.

1. Introduction

Glycosaminoglycans (GAGs) are linear polysaccharides, which are major components of the extracellular matrix (Ricard-Blum et al., 2024). They include Heparan Sulfate (HS), Heparin (Hep), Chondroitin Sulfate (CS), Dermatan Sulfate (DS), Hyaluronic Acid (HA) and Keratan Sulfate (KS). With the exception of HA, GAG chains are found attached to a protein core to form a proteoglycan (PG). GAGs exhibit various interactions with proteins, growth factors, cytokines, and chemokines, facilitated by electrostatic forces influenced by sulfation patterns along their chains. Sulfation patterns of GAGs are not genetically encoded but are regulated by the spatiotemporally controlled expression of enzymes involved in the GAG biosynthesis machinery, including glycosyltransferases, sulfotransferases and epimerases (Annaval et al., 2020). As a result, GAGs modulate diverse biological processes and contribute significantly to tissue homeostasis (Chen et al., 2021). Bone Morphogenetic Protein 2 (BMP2) is a protein member of the transforming growth factor beta superfamily (TGFβ) and is a potent osteogenic growth factor, classified also as a morphogen. The transmission of BMP signals from receptors on the plasma membrane to the nucleus occurs *via* the canonical SMAD pathway or several non-canonical pathways (Derynck & Budi, 2019). Extracellular matrix components, such as GAGs and adhesion proteins, can spatially and temporally regulate the BMP2 signaling cascade (Ramel & Hill, 2012; Umulis, O'Connor, & Blair,

* Corresponding authors.
E-mail addresses: romain.vives@ibs.fr (R.R. Vivès), elisa.migliorini@cea.fr (E. Migliorini).

https://doi.org/10.1016/j.carbpol.2024.122294
Received 25 March 2024; Received in revised form 7 May 2024; Accepted 17 May 2024
Available online 24 May 2024

2009).

Regarding GAGs, alterations in the biosynthesis of HS, due to the mutation of exostosin (EXT) genes, are responsible for Hereditary Multiple Osteochondromas (HMO) (Jones et al., 2010; Matsumoto, Irie, Mackem, & Yamaguchi, 2010; Wuyts et al., 1998) a skeletal disease in humans characterized by an altered BMP2 signaling (Huegel et al., 2013; Inubushi, Nozawa, Matsumoto, Irie, and Yamaguchi, n.d.). CS proteoglycans (PGs) may also contribute to bone tissue homeostasis by regulating BMP2 signaling. Although there is limited research on the involvement of CS in BMP signaling, it has been demonstrated that a defect in the CS sulfation pattern in mice results in a severe chondrodysplasia (Klüppel, Wight, Chan, Hinek, & Wrana, 2005). This mutation also leads to a significant decrease of BMP signaling. We therefore hypothesize that both HS and CS play a role *in vivo* in maintaining BMP signaling homeostasis.

While the lack of HS is dysregulating the embryonic development and BMP signaling, several contradictory findings have obscured their precise role as promoter or inhibitor of signaling. Takei and coworkers showed that the signaling of hedgehog (Hh), Dpp (homolog of BMP in Drosophila) and wingless morphogens is reduced in cells mutant for drosophila homologs of EXT genes, indicating a positive role of HS in these signaling pathways. Several studies contradict these results and report a negative role of HS in BMP signaling (Fisher, Li, Seghatoleslami, Dealy, & Kosher, 2006; Mundy, Yang, Takano, Billings, & Pacifici, 2018). Huegel and coworkers showed that reducing EXT1 expression or interfering with HS function by heparinase I or Surfen treatment stimulated the chondrogenesis *in vivo*, with an increase of pSMAD1/5/9 protein levels and Runx2/Sox9 gene expression (Huegel et al., 2013). We believe that the comparison of these studies is complicated by several factors that may influence the effect of GAGs in these experiments, such as the location (extracellular/cell-surface) of GAGs, the presentation mode of BMPs (solution/immobilized), the assay duration (short-term/long-term), or even the concentrations of growth factor or GAG used (Le Pennec, Picart, Vivès, & Migliorini, 2023). We conclude that the precise role of GAGs in BMP signaling, therefore, remains unclear.

The understanding of GAGs-protein interactions is a pivotal step to comprehending the complete picture of the GAG-mediated regulation of protein bioactivity. Regarding BMP2, it exhibits a well-demonstrated high affinity for HS (Billings, Yang, Mundy, & Pacifici, 2018; Migliorini et al., 2017) and Hep (Kisiel et al., 2013; Ruppert, Hoffmann, & Sebald, 1996; Siverino et al., 2023). However, the affinity values described in the literature deserve to be clarified since they are subject to variations of several orders of magnitude, likely related to different experimental setups or GAG sources. The sulfation degree and sulfation patterns of HS are critical structural features driving the high affinity of HS for various proteins. For some proteins like antithrombin III and FGF2, specific sulfation motifs and/or sulfation sequences of HS are particularly important for their interaction and their bioactivity (David A. Pye, Vives, Turnbull, Hyde, & Gallagher, 1998; Richard, Swanson, & Olson, 2009). In the case of BMP2, few studies investigated the HS sulfation motifs or sequences required for the interaction. Using desulfated Hep, Smith et al. demonstrated that N-sulfation was more important for BMP2 binding compared to 6-O sulfation and 2-O sulfation, which had a minor contribution (Smith et al., 2018). This trend is, however, in contradiction with *in vitro* assays of Tellier and coworkers, who showed a minor importance of N-sulfation and a role of 6-O sulfation using desulfated Hep immobilized on microparticles (Tellier, Miller, McDevitt, & Temenoff, 2015). Chopra and coworkers also studied the HS-BMP2 interaction with a microarray displaying 3-O sulfated hexasaccharides. The authors demonstrated that BMP2 bound more strongly on oligosaccharides including a 3-O sulfate. They noticed generally a high affinity of several proteins to oligosaccharides with a central IdoA (2*S*)-GlcNS(3S6S) disaccharide (Chopra et al., 2021). In zebrafish, 3-O sulfation was demonstrated to contribute to the spatial restriction of BMP signaling away from ventricular myocytes, thereby promoting the cardiac contractile function (Samson et al., 2013). In contrast, in a microarray study, Söderlund and coworkers did not observe significant modification of BMP interactions for five distinct oligosaccharides, with K_D values in the 100 nM range. In particular, an HS dodecasaccharide including a 3-O sulfated GlcNS(3*S*6*S*)-IdoA(2*S*) sequence did not have a specific effect. In more recent studies, a synthetic HS with a controlled sulfation pattern has been used to enhance the bioactivity of BMP2 (Shaffer et al., 2024). However, it remains unclear whether BMP2 requires a specific sulfation sequence within the HS chain for high affinity binding.

In this study, we have examined the molecular interactions between various GAGs and BMP2, yielding novel insights into their affinity and kinetics parameters. To investigate the involvement of GAGs in mediating BMP2 signaling as extracellular components, we employed biomimetic streptavidin (SAv) platforms, previously developed to support cell adhesion and present immobilized GAGs in a manner resembling the natural extracellular matrix (Sefkow-Werner et al., 2020; Thakar et al., 2017). These platforms have been thoroughly characterized regarding the binding of GAGs and BMP2 and the co-functionalization with cRGD peptides. To explore the role of cell-surface GAGs, we employed different CHO cellular models, carrying mutations of GAG biosynthesis enzymes. In particular, we unveil novel perspectives about the distinct contributions of cell-surface HS and cell-surface CS in BMP2 signaling. Finally, we generated a library of HS tetrasaccharides and hexasaccharides to investigate the structural specificities of BMP2-HS binding and the significance of specific HS sulfation motifs and sequences. Moreover, we performed 3D molecular reconstruction and molecular dynamics simulations to gain a deeper understanding of these interactions.

2. Materials and methods

2.1. Buffers and molecules

A solution called Hepes, with a composition of 10 mM Hepes and 150 mM NaCl (Sigma-Aldrich) at pH 7.4, was used for diluting and rinsing all molecules unless otherwise specified. mPEG-Thiol and biotin-PEG-Thiol (11156-0695 and 41156-1095, Polypure) were functionalized on a gold substrate and further conjugated with streptavidin (SAv, Sigma-Aldrich). Refer to previous works for information on the biotinylated cyclic arginyl-glycyl-aspartic acid (cRGD) (Sefkow-Werner et al., 2020; Thakar et al., 2017). Heparan sulfate (HS) sourced from porcine intestinal mucosa was acquired from Celsus Laboratories. It has an average molecular weight of 12 kDa and a polydispersity of 1.59 (Mulloy et al., 1997). Chondroitin Sulfate A (C9819, CS-A, bovine trachea, average molecular mass 28 kDa (Hamad et al., 2008)) and Dermatan Sulfate (C3788, DS/CS-B, porcine intestinal mucosa) were purchased from Sigma-Aldrich. Chondroitin Sulfate D (400676, CS-D, shark cartilage, average molecular mass of 38 kDa (Djerbal et al., 2019)) was acquired from Seikagaku. Chondroitin Sulfate E (CS-E) and Hyaluronic Acid (HA) were gifts from Kawthar Bouchemal. BSA was purchased from ThermoFisher Scientific (BP9703-100) and D-(+)-Trehalose was acquired from ThermoFisher Scientific (A19434.14). BMP2 produced in CHO cells was obtained from Medtronic (26 kDa, InductOs). Heparinase I, II and III were acquired from GrampEnz (GE-H0001, GE-H0002, GE-H0003). Filtered phosphate buffered saline (PBS, without $MgCl_2$ and $CaCl_2$, Gibco™, ThermoFisher Scientific) was used in all the rinsing steps related to the cells.

2.2. Generation of HS-oligosaccharide libraries

As previously described, an HS-oligosaccharide library was generated (Pye, Vivès, Hyde, & Gallagher, 2000), by digesting HS chains with Heparinase III. Heparinase III was selected for its cleavage specificity for GlcNAc-GlcA linkages, enabling the release of intact N-sulfated oligosaccharides. For this, HS (8 g) was exhaustively digested with

heparinase III at 37 °C in 100 mM sodium acetate and 0.5 mM $CaCl_2$ buffer at pH 7.1 heparinase buffer. The digestion was monitored for 6 days by absorbance measurements at 232 nm. Digestion products were then separated by Bio-Gel P-10 (Bio-Rad) size-exclusion chromatography (44*1500 mm) equilibrated in 0.2 M NaCl solution at a flow rate of 0.5 mL/min. Following measurement of absorbance at 232 nm, Fractions (15 mL) corresponding to size-defined oligosaccharides were collected, pooled, dialyzed against water (Spectra/Por 1 kDa tubing) and lyophilized. The dp4- and dp6-oligosaccharides were then separated according to their charge by strong anion exchange (SAX)-HPLC using a ProPac PA1 preparative column (ThermoFisher Scientific) equilibrated in H_2O pH 3.5. For each size defined fraction, the salt gradient was optimized to resolve the different oligosaccharide species.

2.3. Analysis and characterization of HS-oligosaccharides

As the generated HS-oligosaccharide libraries included a large number of species, with great disparities in the quantities obtained and purity achieved, characterization was achieved by reverse phase ion pair (RPIP)-HPLC disaccharide analysis, as described previously (Laguri, Sadir, Gout, Vivès, & Lortat-Jacob, 2022). For this, oligosaccharides were exhaustively digested using a mix of heparinase I, II and III (10 mU each) in heparinase buffer for 48 h at 37 °C. Disaccharide products were then analyzed by RPIP-HPLC on a C18 column (Luna 5 μm C18, 4.6 × 300 mm, Phenomenex), using a NaCl gradient in 1.2 mM tetra-N-butylammonium hydrogen sulfate (TBA), pH 3.15, 8.5 % (v/v) acetonitrile, followed by post-column derivatization using 0.125 % 2-cyanoacetamide and 0.5 % NaOH and fluorescence measurement (excitation 346 nm, emission 410 nm). Disaccharide composition was determined following calibration of the data with commercial HS disaccharide standards (Iduron, Alreley Edge, UK: ΔUA–GlcNAc/ΔUA–GlcNS /ΔUA–GlcNAc6S /ΔUA2S – GlcNAc /ΔUA – GlcNS6S /ΔUA,2S – GlcNS /ΔUA,2S – GlcNAc,6S /ΔUA2S – GlcNS6S). The analysis was repeated after $NaBH_4$ reduction to determine the reducing-end disaccharide of oligosaccharides, which could not be derivatized anymore. Oligosaccharides were reduced with 50 mM NaOH and 150 mM $NaBH_4$ (Sigma-Aldrich) overnight at 37 °C, followed by pH neutralization with acetic acid (Sigma-Aldrich). Reduced oligosaccharides were then digested with heparinases prior to RPIP-HPLC analysis.

2.4. Biotinylation of GAGs and oligosaccharides

Glycosaminoglycans or oligosaccharides were incubated for 24 h at 37 °C at 5 mg/mL concentration in 100 mM sodium acetate pH 4.5, 12.5 nM EZ-Link Alkoxyamine-PEG4-biotin (ThermoFisher Scientific), and 10 mM aniline (Sigma-Aldrich) to achieve coupling with the biotinylated linker. Double HiTrap® Desalting columns (GE29-0486-84, Sigma-Aldrich) coupled to AKTA Pure equipment (GE Healthcare) were used to identify and recover the fractions of desalted biotinylated GAGs. The compounds were next concentrated by freeze-drying.

2.5. Bio-layer interferometry (BLI) measurements

BLI studies were performed with an OctetRED96e instrument (Pall/FortéBio), using the manufacturer's software (Data Acquisition v11.11) to record the data, as previously described (Diaz-Salmeron et al., 2021; Khodr, Machillot, Migliorini, Reiser, & Picart, 2021). Briefly, all molecules were resuspended in PBS, 0.02 % Tween® 20 (PBS-T). Samples were deposited in a black 96 plates (Nunc F96 MicroWell, ThermoFisher Scientific), kept at a constant temperature of 25 °C, and stirred at 1000 rpm throughout the experiments. All biosensors were pre-wetted in 200 μL of PBS-T for 10 min before each test, after which the equilibration was monitored for 60 s. SAv-coated biosensors (FortéBio) were loaded with each biotinylated GAG ligand for 600 s. The concentrations used for immobilization were 0.06 μg/mL and 0.12 μg/mL for HS and CS/DS/HA, respectively. The concentrations used were 0.075 μg/mL and 0.04 μg/mL for dp4 and dp6 ligands, respectively. Association and dissociation phases were monitored during 200 s. Identical procedures were followed on non-functionalized reference biosensors to assess and monitor BMP2 non-specific binding. All measurements were performed in three independent experiments, with new sensors and newly prepared sample solutions.

Kinetics data were analyzed using the manufacturer software (Data analysis HT v11.1). The non-specific signals on reference biosensors were subtracted from those obtained on GAGs-functionalized biosensors for each BMP2 analyte concentration. The kinetic signals were then fitted using a global method with a 1:1 Langmuir model. Dissociation on several GAG ligands comprised a rapid and slow phase close to the baseline. Therefore, only the first 40 s of dissociation were included in the fitting. Affinity constants were calculated from the ratio of k_{off}/k_{on} values. The reported values are plotted as mean ± SEM obtained from independent experiments.

2.6. Biomimetic streptavidin platforms surface functionalization

The preparation of biomimetic SAv platforms is detailed elsewhere (Sefkow-Werner et al., 2020). The assembly of SAv platforms was achieved by a liquid-handling robot executing all the incubation and rinsing steps as described in previous work (Sefkow-Werner et al., 2022). SAv was incubated at 10 μg/mL for 30 min to construct a monolayer, and a 2-hour blocking with 10 % BSA and 0.6 M of D-(+)-Trehalose (Le Pennec et al., 2024) was achieved to reduce non-specific binding of BMP2. Then, co-functionalization of cRGD and GAGs was performed with a 10-min incubation of biotinylated cRGD at 1.2 μg/mL before saturation of SAv binding sites with biotinylated GAGs at ten μg/mL for 40 min. BMP2 was allowed to bind to GAGs with a 90-min incubation step at 0.02 μg/mL (0.768 nM) in Hepes supplemented with 0.02 % Tween® 20 (Hepes-T) to prevent aggregation at physiological pH during the process. To remove the non-adsorbed BMP2, two rinsing steps were performed in Hepes-T and three rinsings in Hepes before cell seeding.

2.7. Ex situ characterization with quartz crystal microbalance with dissipation monitoring (QCM-D)

We measured with QCM-D (QSense Analyzer, Biolin Scientific) the shifts in resonance frequency (Δf in Hz) and energy dissipation (ΔD in dissipation units, ppm = 10^{-6}) to characterize binding events in the biomimetic platforms sequential buildup as detailed elsewhere (Migliorini et al., 2017). To enable adequate signal detection for comparing its binding on various GAGs, BMP2 was injected at a concentration of 5 μg/mL. Molecules were injected into the liquid chamber with a peristaltic pump (IPC4, Ismatec) imposing a flow rate of 15 μL/min until saturation (except for cRGD and BMP2), followed by rinsing with Hepes at the same flow rate. For cRGD and BMP2, we used a "fast injection" procedure to mimic the functionalization performed by the liquid-handling robot. The solutions of cRGD and BMP2 were injected at a high flow rate of 100 μL/min until the liquid chamber was filled. The flow was stopped at this moment to let the molecules bind in a static regime. All measurements of frequency and dissipation shifts were performed after the stabilization of the signal. For co-functionalization of cRGD with GAGs, the frequency shift of −4.7 Hz obtained for a 10 mi static incubation at 1.2 μg/mL was reproduced under flow using 0.5 μg/mL of cRGD to allow better control.

2.8. Cell culture

CHO cell lines (CHO-K1: CCL-61™; pgsD-677: CRL-2244™; pgsA-745: CRL-2242™) were cultured below confluence in polystyrene cell culture flasks (Falcon®, Corning) using growth medium composed of Dulbecco's modified Eagle's medium (DMEM/F-12 GlutaMAX, 10565018, Gibco™), supplemented with 10 % heat-inactivated fetal bovine serum (FBS, 10270-106, Gibco™), and 1 % of antibiotic-

antimycotic (15240062, Gibco™). Cells were cultured at 37 °C under a 5 % CO_2 atmosphere until they were discarded upon reaching a passage number of 12. Before any experiment, cells were serum-starved for 4 h. Accutase (A6964, Sigma-Aldrich) was used to detach the cells from the culture flasks, and they were seeded on functionalized surfaces in a growth medium without FBS. The seeded cells were maintained at 37 °C with 5 % CO2 throughout the experiment.

2.9. Cellular assays on biomimetic platforms

10,000 starved cells were seeded in 96-well plates functionalized with biomimetic platforms for each condition. The soluble BMP2 (sBMP2) positive control consisted of seeding cells with 0.1 μg/mL BMP2 on platforms with cRGD. For other conditions, we focused on the role of adsorbed BMP2 on the GAGs by rinsing the unbound BMP2 before seeding cells. Cells were fixed after 90 min with pre-fixation and fixation steps using 2 % Paraformaldehyde (PFA) for 5 min and 4 % PFA for 20 min, respectively. Each condition was assessed with intra-experimental technical duplicates and at least biological triplicate.

We adapted already published protocols to quantify pSMAD1/5/9 *via* IF (Sales et al., 2022; Sefkow-Werner et al., 2022). Cells were imaged using InCell Analyzer 2500 using the 20× objective on three channels. Images were further analyzed with the automated image analysis software InCarta (Molecular Devices), as previously described (Sefkow-Werner et al., 2022): pSMAD1/5/9 intensity was measured only inside the nucleus under a mask defined by the DAPI signal and background-subtracted for at least 100 cells/well. The mean nuclear area was calculated by the InCarta software. The mean intensity was calculated for comparing conditions with identical nuclear areas. In contrast, the total intensity in the nuclei was plotted for conditions exhibiting differences in the nuclear area.

2.10. Molecular dynamic simulations

Initial coordinates of BMP2 were set up according to the X-ray structure (PDB: 6omn), and the missing 11 residues of N-terminal ends were constructed de-novo using AlphaFold2 (Jumper et al., 2021). Available online: https://alphafold2.biodesign.ac.cn/.

Computer simulations were performed in four steps:

First, to obtain the initial orientation of HS-fragment (dp4) concerning the protein, molecular docking was performed using the ClusPro server (Mottarella et al., 2014). Considering the high flexibility of the N-terminal ends, implying some uncertainty in their instantaneous geometry and orientation, the first 11 residues of each protein subunit were truncated for the docking procedure.

Second, the stability of the binding poses determined by docking was verified in the course of molecular dynamics (MD) with HS of the increased oligosaccharide length up to those used in the experiment, dp6 (1 μs long trajectories).

Third, the binding of HS-fragment to the full-length protein was explored. HS's initial orientation was kept as in the most stable complex obtained at the second step of simulations. The N-terminal ends of BMP2 were oriented randomly but did not interact with the HS fragment.

To enhance the conformational sampling of N-terminal ends, accelerated MD (aMD) was used. In AMD, a positive bias potential is added to the potential energy of the simulated system when it is below threshold energy. The threshold energy was determined based on the energy of dihedral angles calculated along the conventional MD trajectory of the protein. The arbitrary acceleration parameter was selected to meet two conditions: increase the non-structured ends' flexibility and not disturb the folding of the globular part of the protein.

The structures of the complexes were diversified by exploring the orientation of the ligand in the binding site. The HS fragment was rotated along its longitudinal and transverse axes by 180 degrees, resulting in four complex structures for one ligand. In total, the complexes with two different patterns of HS sulfation from the panel of the ligand used in the BLI experiment, namely I and J, were simulated, resulting in eight complexes. To compare the binding modes and energies of I and J directly with BMP2, the initial structures for the J were derived from the equilibrated structures of the complexes of BMP2 with the I. To this end, the position of one of the sulfate groups was modified. Then, complexes of BMP2 with J were equilibrated in the course of aMD trajectories.

Fourth, the complexes formed during aMD trajectories were equilibrated during short conventional MD trajectories.

All MD and aMD trajectories were calculated using the AMBER18 program package with AMBER14SB force field for protein and GLYCAM 06j-1 force field for HS fragments. The protein or the complex was placed into a water box with periodic boundary conditions. The rectangular box was generated with borders at a distance of >10 Å from any residue of the protein-HS complex and filled with water molecules using the "tleap" module of the AMBER18 program. The periodic boundary conditions in x,y, and z dimensions were applied during MD simulations. The TIP3P model was used for water molecules. Sodium ions were added to neutralize the charge of the molecular system.

The integration step of 2 fs was used with the SHAKE algorithm (Ryckaert, Ciccotti, & Berendsen, 1977). For long-ranged electrostatic interactions, the Particle mesh Ewald (PME) method was employed (Essmann et al., 1995). The simulations were carried out in the isotherm isobar thermodynamic ensemble. The temperature (300 K) and the pressure (1 bar) were kept constant using a Langevin thermostat with a collision frequency of 2 ps^{-1} and a weak coupling algorithm with a relaxation time of 2 ps, respectively. First, the system was minimized for 5000 steps and then equilibrated. In the MD production run, 200 ns of the trajectory were accumulated. The length of aMD production trajectories varied from 400 to 1200 ns. The binding energies were calculated using the Molecular Mechanics with Generalized Born and Surface Area Solvation (MM/GBSA) approach.

2.11. Statistical analysis and data treatment

To compare independent experiments, the values were possibly normalized to positive control, the mean was calculated, and the SEM was used for the error bars in the figures and the text (mean ± SEM). For cell experiments, intra-experimental technical duplicates were used to calculate each condition's mean of biological replicates. The significance between the two conditions was tested with the non-parametric Mann-Whitney test and represented in the graphs with $*p \leq 0.05$.

3. Results

3.1. BMP2 exhibits higher binding affinity for HS compared to CS, DS and HA

The binding affinities between BMP2 and GAGs are highly variable in the literature and have never been compared within the same study. Here, we have investigated the dynamics of the interactions between BMP2 and different GAGs (HS, HA, CS-A, -D, -E and DS) using the BLI biophysical characterization technique. As depicted in Fig. 1A–E and Fig. Si1, the binding of BMP2 was detected on all the different GAGs except the non-sulfated HA. BMP2 at low concentration (10 nM) bound to HS, whereas the binding to CS or DS required BMP2 concentrations above 200 nM to trigger a detectable signal. CS-A exhibited the lowest binding affinity to BMP2, requiring concentrations >600 nM. We determined binding affinities (K_D) and k_{on} and k_{off} kinetics parameters for the tested GAGs by fitting the binding curves with a 1:1 binding model (Fig. 1F and Fig. Si1). BMP2 bound to HS with the highest affinity (K_D of 57 ± 7 nM) followed by CS-D (K_D of 400 ± 43 nM). The other CS types and DS exhibited affinities in the low μM range (2.5 ± 0.4 and 1.4 ± 0.4 μM for CS-E and DS, respectively) or above 70 μM for CS-A. Considering the excessive amounts of BMP2 required to precisely determine the affinity of the weakest interactions (>1 μM), the K_D values

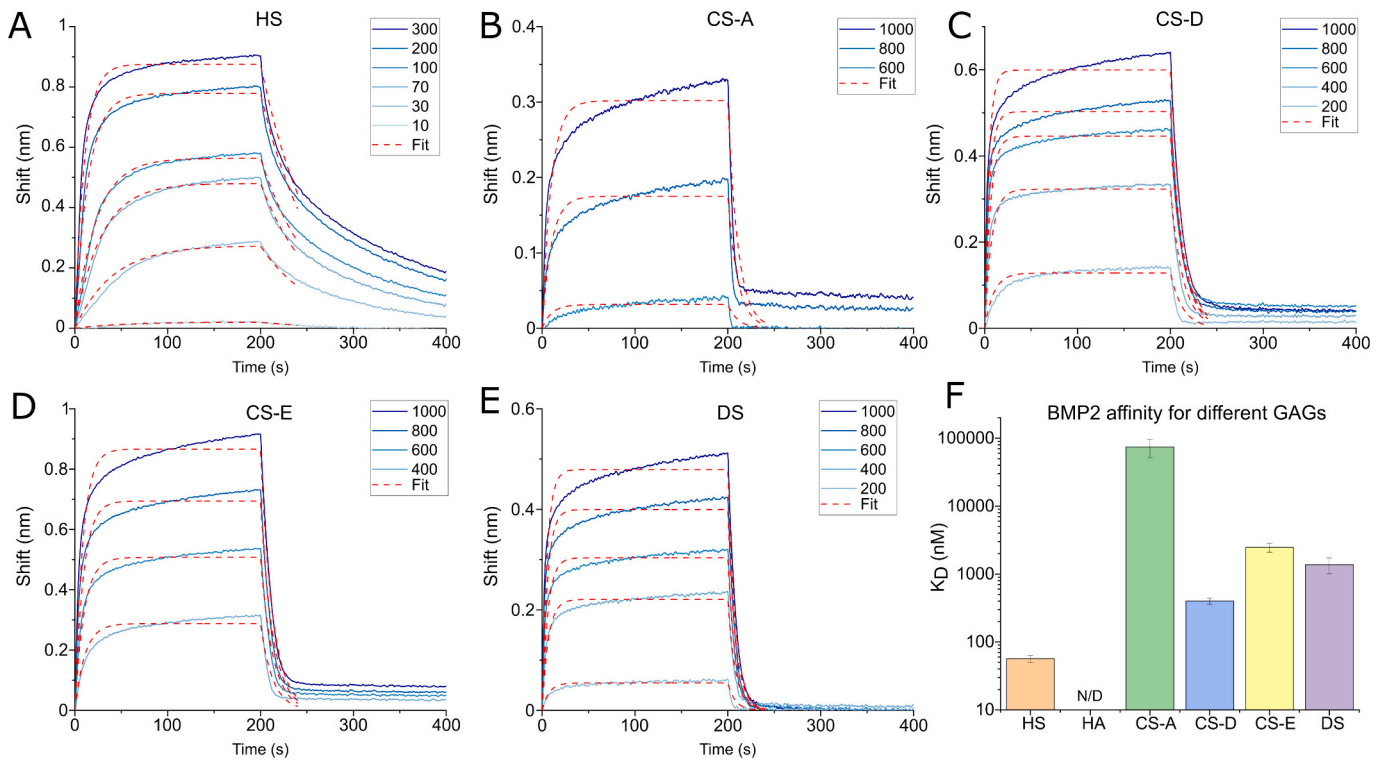

Fig. 1. Biolayer Interferometry (BLI) kinetics assays of BMP2 binding on different GAGs: A. HS; B. CS-A; C. CS-D; D. CS-E; E. DS. The BMP2 association and dissociation phases were measured for 200 s each at different concentrations indicated at the bottom of each graph (nM). The curves were fitted with a 1:1 Langmuir binding model on the entire association and 40 s of the dissociation (red curves) to obtain the kinetics parameters of the interactions. F. K_D values of BMP2 interactions for the different GAGs, representing the inverse of the affinity, are plotted on a logarithmic scale.

for CS-E, DS, and CS-A may lack accuracy compared to HS and CS-D, as the BMP2 concentration range employed for these compounds was not optimal.

3.2. Design of well-characterized biomaterials for cellular assays

Once the BMP2 affinity for different GAGs was determined, we sought to investigate the role of GAGs in BMP signaling, which has been the subject of conflicting studies (Fisher et al., 2006; Huegel et al., 2013; Inubushi et al., n.d.; Kuo, Digman, & Lander, 2010; Lin et al., 2000; Takei, Ozawa, Sato, Watanabe, & Tabata, 2004). These discrepancies may be attributed to differences in GAG presentation mode (in solution or bound to a biomaterial) and their location (cell-surface or extracellular). To address this, we adapted our previously developed biomimetic SAv platforms, which enable the presentation of GAGs as extracellular components mediating the BMP2 cellular response (Sefkow-Werner et al., 2020; Sefkow-Werner et al., 2022). Gold has been chosen as support, on which a biotin-PEG-thiol linker binds an SAv monolayer. Biotinylated GAGs are then immobilized on SAv, and BMP2 is adsorbed onto the GAG films. The functionalisation process was characterized *ex-situ* with QCM-D to evaluate the binding of each GAG and BMP2 to the platforms, as exemplified for HS and CS-D in Fig. 2A–B. The binding of the SAv monolayer was homogeneous in all experiments, with an average shift around -24.3 ± 1.3 Hz. The immobilization of GAGs on the SAv monolayer generates important positive shifts in dissipation, indicating an increased softness of the platforms and strong negative frequency shifts due to the high hydration of the GAG layer (Migliorini et al., 2015). The immobilization of HA yielded the largest frequency shift (thus the heaviest hydrated mass on the QCM-D crystals), CS/DS compounds yielded intermediate shifts and HS the smallest shift (Fig. 2C, E). This trend was also observed in the analysis of GAGs by acrylamide gel electrophoresis (Fig. Si2), confirming the distinct molecular weights of these GAGs. Subsequently, the binding of BMP2 at five µg/mL was varying depending on the GAGs, as indicated by the distinct frequency shifts (Fig. 2D, F). BMP2 bound more to CS-D, followed by CS-E, with frequency shifts of 23.7 ± 3.9 Hz and 16.9 ± 3.6 Hz, respectively. The frequency shift for DS was larger than for HS and CS-A, with values of 14.2 ± 4.2 Hz, 12.8 ± 0.7 Hz, and $10.1 + 2.1$ Hz, respectively. On the contrary, BMP2 did not bind to the non-sulfated HA. The binding of BMP2 on CS seems less stable than on HS since some BMP2 dissociated during the rinsing (Fig. Si3A).

As previously observed, the binding of BMP2 to HS triggered a negative shift of the dissipation, likely indicating a cross-linking of HS chains mediated by the growth factor (Migliorini et al., 2017). We show that BMP2 binding on CS and DS triggers the same effect, characterized by a negative dissipation shift measured *via* QCM-D (Fig. 2H, J). By plotting Δf *versus* ΔD, we can relate the levels of BMP2 binding (Δf) to the rigidification of the GAG film (ΔD). As shown in Fig. Si3B–C, we observed that for similar Δf induced by BMP2, the cross-linking is stronger for HS and DS, followed by CS-E and CS-A, and finally, CS-D.

For cellular assays, the biomimetic platforms were co-functionalized with cRGD peptide to mediate a similar cell adhesion for the different GAG conditions. The co-functionalization process of cRGD with HS, CS-A or CS-D was also characterized *via* QCM-D, as shown in Fig. Si4. In conclusion, we obtained well-characterized platforms binding and presenting cRGD, GAGs and BMP2 for cellular studies.

3.3. Role of extracellular and cell-surface GAGs in BMP2 signaling

To explore the potential functional differences between cell-surface (csGAGs) and extracellular GAGs in BMP2 signaling, we seeded CHO cells on characterized biomimetic SAv platforms. We adopted either wild-type (WT) or mutant CHO cells presenting an altered repertoire of cell surface GAGs. We first investigated the role of extracellular GAGs on BMP2 bioactivity. CHO WT cells were cultured on biomimetic platforms for 90 min and fixed, and the nuclear pSMAD1/5/9 was measured by IF

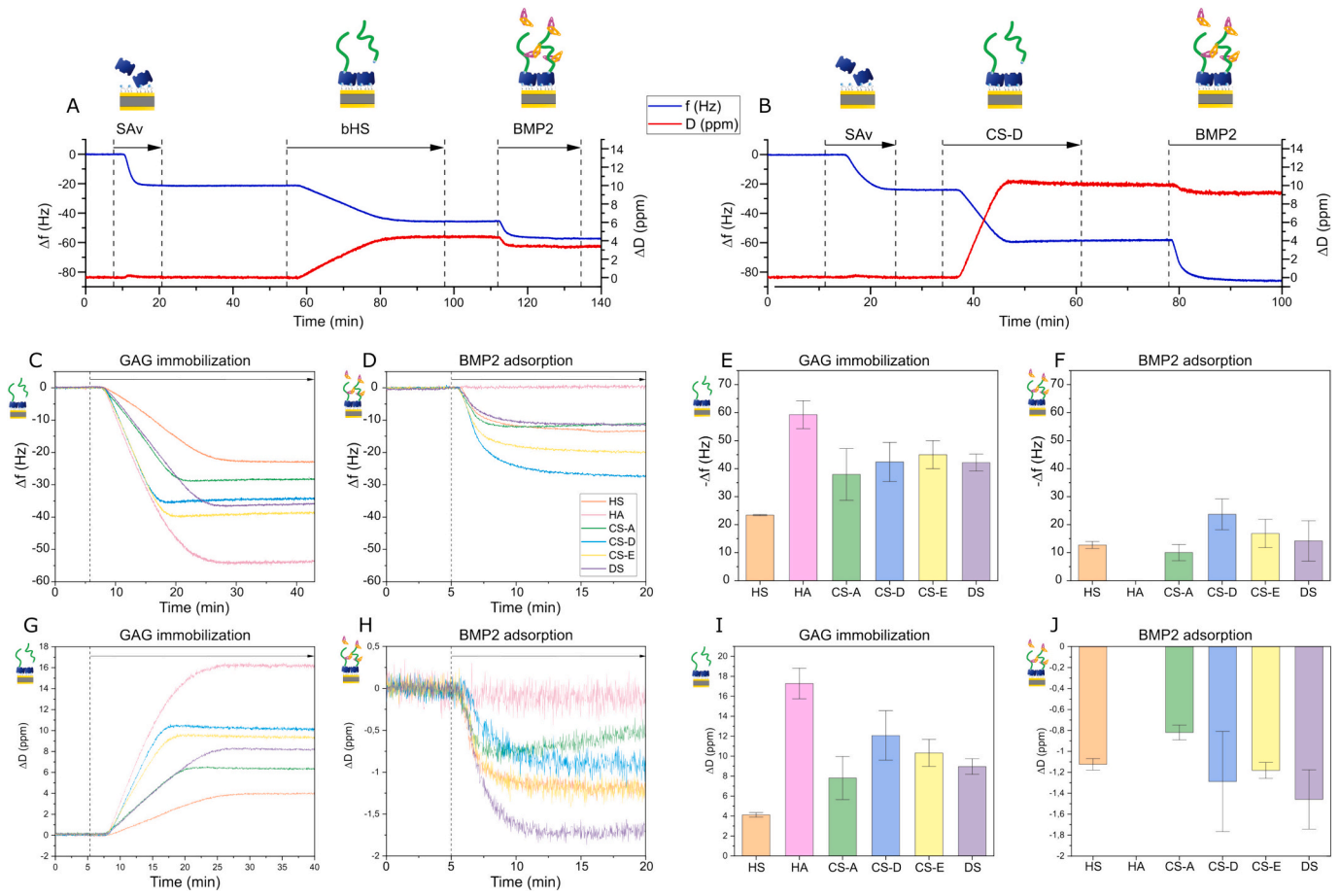

Fig. 2. Characterization of the sequential buildup of the biomimetic platform by QCM-D. Example of platform buildup characterized by QCM-D for A. HS and B. CS-D. Black arrows represent the injection of molecules, SAv, biotinylated GAGs and BMP2, alternating with Hepes rinsing. The third overtones of frequency and dissipation measurements are depicted in blue and red, respectively. The overlapped curves showing the immobilization of all GAGs on SAv are shown in panels C. frequency and G. dissipation. Similarly, the binding of BMP2 to GAGs is shown on panels D. frequency and H. dissipation. The experiments were performed at least in duplicate for each GAG, and we quantified the mean of frequency shifts (E–F) and dissipation shifts (I-J) for GAG immobilization (E, I) and BMP2 binding (F, J). Data are plotted as mean ± SEM.

(Fig. 3A). The mean nuclear intensisty of pSMAD1/5/9 is plotted in Fig. 3B. We show that only HS significantly increased the amount of pSMAD1/5/9 above the control. CS-D seemed to generate a more pronounced signal than DS and the other CS types, but these differences were not significant. These data correlate well with the affinity measured by the BLI experiment: the higher the binding affinity, the stronger the BMP-induced SMAD1/5/9 phosphorylation. We first noticed significant non-specific binding of BMP2 to the platforms during method development. This non-specific binding was not strongly detected by QCM-D (Migliorini et al., 2017), suggesting that only a small amount of BMP2 binds non-specifically to the platforms. Nevertheless, even these small amounts can trigger SMAD1/5/9 phosphorylation, therefore complicating the interpretation of the results. In the following experiments, we succeeded in reducing the non-specific binding by blocking the substrate with BSA and trehalose (Le Pennec et al., 2024).

To test the role of the csGAGs, we analyzed CHO with defects in the GAG synthesis. We used the wild-type CHO-K1 and mutant CHO pgsD-677 and pgsA-745 cell lines previously characterized. Wild-type CHO-K1 (CHO WT) cells produce about 70 % HS and 30 % CS (Lidholt et al., 1992), whereas CHO pgsD-677 cells (CHO KO HS) contain mutations in the gene encoding EXT1, an enzyme responsible for HS chain elongation (Wei et al., 2000). We quantified that these cells produce 6 fold more csCS than the wild-type cells (Fig. Si5A). CHO-pgsA-745 cells (CHO KO HS/CS) completely lack csHS and csCS since they are deprived of xylosyltransferase responsible for the catalysis of the first sugar transfer in GAG synthesis (Esko, Rostand, & Weinke, 1988; Esko, Stewart, & Taylor, 1985; Lidholt et al., 1992). In Fig. 3C–D, the total pSMAD1/5/9 levels induced by soluble BMP2 treatment were evaluated for the three CHO variants exhibiting distinct cell-surface GAGs. As previously shown (Huegel et al., 2013; Inubushi et al., n.d.), we noticed increased SMAD1/5/9 phosphorylation for the CHO KO HS compared to the wild type, even after subtraction of the basal expression of pSMAD1/5/9 in these cells (Fig. Si5B). Interestingly, the CHO KO HS/CS cells deprived of csGAGs exhibited a pSMAD1/5/9 level similar to the wild type cells. These results obtained with IF were also confirmed by Western Blot (Fig. Si5C–D). Overall, HS mutant cells exhibit an increased pSMAD1/5/9 level while HS/CS mutants display reduced signaling. These results suggest that csCS promotes BMP2 signaling while csHS may have an inhibitory effect. On the contrary, extracellular HS enhances pSMAD1/5/9 levels compared to HA, CS and DS.

3.4. *Heparan sulfate structural requirements for BMP2 binding*

Since we have shown that HS is the most potent extracellular GAG to induce the BMP-mediated SMAD1/5/9 phosphorylation, immobilized HS on implants might be an attractive target for regenerative medicine. However, the specific sulfation pattern required to bind BMP2 is not known. To receive insight into the interaction with differently sulfate HS structures, we generated a library of HS oligosaccharides, using porcine intestinal mucosa HS as starting material. Because of the tremendous

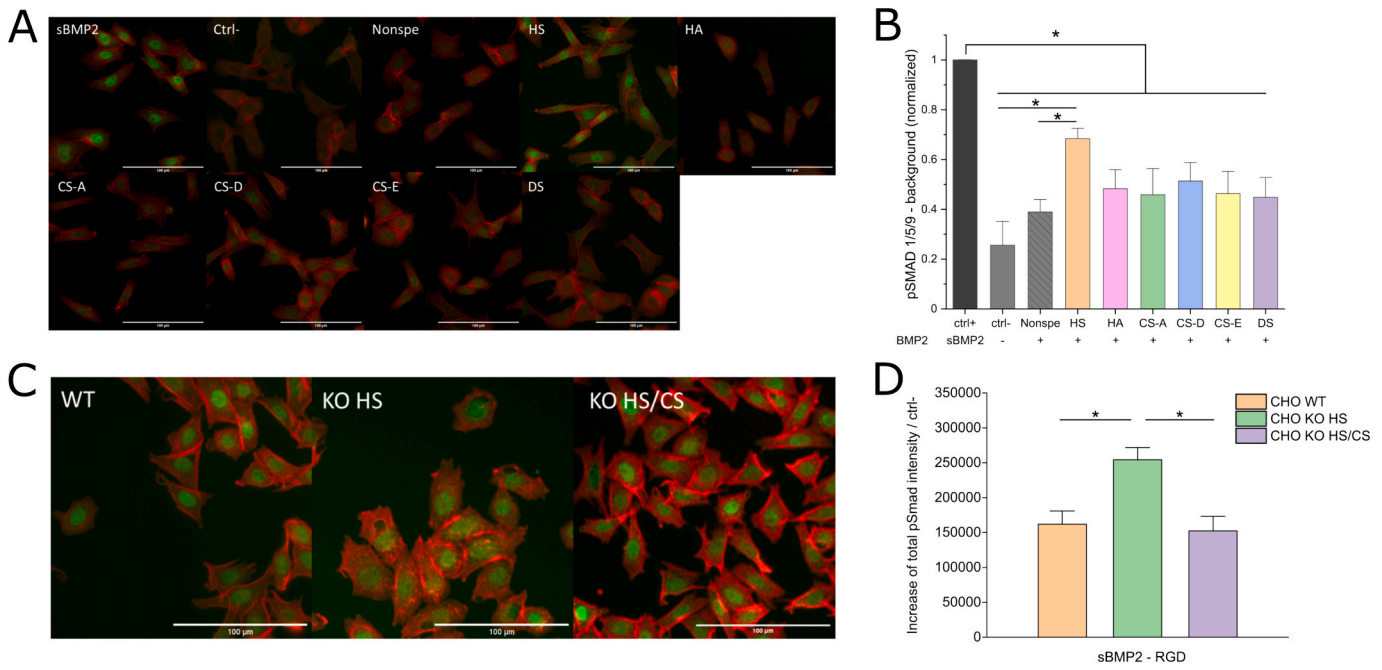

Fig. 3. Extracellular HS enhances while cell-surface HS regulates SMAD1/5/9 phosphorylation, and csCS promotes short-term signaling.
A. Representative IF images of wild-type CHO cells after a 90-min culture on the biomimetic platforms functionalized with different GAGs (extracellular) and BMP2 and stained for actin (red) and pSMAD1/5/9 (green). The scale bar is 100 µm. Positive and negative controls correspond to cRGD functionalized platforms (without GAGs) exposed to soluble BMP2 at 0.1 µg/mL (sBMP2) or not (ctrl-). The platforms harboring GAGs were incubated with 0.02 µg/mL BMP2, which was rinsed before cell seeding. cRGD platforms without GAGs followed the same procedure as control of BMP2 non-specific binding (Nonspe). B. Corresponding mean fluorescence intensity of nuclear pSMAD1/5/9 in wild type CHO cells. Values were normalized by the positive sBMP2 positive control (n = 4). C. Representative IF images of CHO WT, KO HS and KO HS/CS cells cultured for 90 min on cRGD biomimetic platforms with or without sBMP2 at 0.1 µg/mL and stained for actin (red) and pSMAD1/5/9 (green). The scale bar is 100 µm. D. Corresponding total fluorescence intensity of nuclear pSMAD1/5/9 in CHO WT, KO HS and KO HS/CS cells. The intensity value was plotted for each cell type after subtracting the negative control without BMP2 (n = 4). Statistical significance between the two conditions was tested with the Mann-Whitney test and is represented with * for $p \leq 0.05$.

structural diversity of HS, we focused on tetrasaccharides (dp4) and hexasaccharides (dp6) for BMP2 binding studies, which would be the most relevant species for minimal size determination, and would allow isolation of pure enough species to investigate the importance of sulfation patterns. We proved by QCM-D that BMP2 binds to the short dp4, and that dp4-presendted BMP2 can induce pSMAD 1/5/9 phosphorylation (Fig. Si6). After depolymerization with heparinase III, the cleaved fragments were separated by size to obtain pure samples of HS-dp4 and-dp6 (Fig. Si7A). The isolated oligosaccharides were further separated by charge to isolate compounds with distinct sulfation patterns. Fig. 4A (or Fig. Si7B for tetrasaccharides and Fig. Si7C for the full graph of hexasaccharides) shows the resolution of the generated HS-hexasaccharide by SAX-HPLC. Disaccharide analysis of the obtained oligosaccharides was then performed by RPIP-HPLC (Fig. Si8). The oligosaccharides were biotinylated for the most abundant species, and their interactions with BMP2 were analyzed using the BLI technique to determine the K_D parameters. The raw data of the BLI experiment are provided in Fig. Si9. Disaccharide analysis was also performed with $NaBH_4$ oligosaccharide reduction (Fig. Si10) to identify the disaccharide-reducing end (blocked by the reduction), allowing us to determine their sequences with high confidence, as shown in Fig. 4C.

Oligosaccharides tested in BLI comprised between 3 and 6 sulfate groups for hexasaccharides and between 2 and 3 for tetrasaccharides. Some isolated compounds corresponded to a mix of two co-eluting species, which could be individually identified (dp4-AB, dp6-K, -R and -AC, see Fig. 4C). For dp6-G, the relative position of the identified disaccharides could not be ascertained, and the two possible sequences are shown in Fig. 4C. We show for the first time that BMP2 can bind to different HS-dp4 with a moderate affinity (Fig. 4B), in the same range or better than full chains of DS or CS-A,-E. Indeed, the K_D of dp4-S, -Y and -AB compounds for BMP2 was between 500 nM and 1 µM and the K_D of dp4-P was about 3 µM. We also show that the affinity for HS-dp6 oligosaccharides is generally better than for HS-dp4, with some potent BMP2-binding compounds (dp6-Z, -AC) exhibiting an affinity relatively close to that of full chains of HS. By studying the variation in affinity in relation to the oligosaccharide structures more precisely, some binding features could be identified. The dp6-D, -I and -L only differ by adding one consecutive sulfate. While the tri-sulfated dp6-D binding was too weak to measure an affinity, a low affinity was measured on the dp6-I ($K_D = 1143 \pm 472$ nM), showing one additional 2-O sulfate group and a high affinity was determined for the dp6-L ($K_D = 206 \pm 64$ nM) featuring five consecutive sulfate groups (additional 2-O and N- sulfates). These data support the idea that the sulfation degree increases the binding affinity for BMP2. Interestingly, dp6-J showed a 4-fold better affinity ($K_D = 273 \pm 61$ nM) than the structurally close dp6-I exhibiting the same sulfate number, indicating that sulfation patterns are also important for the binding. While dp6-I is composed of four monosulfated monosaccharides, dp6-J differs by featuring a central trisulfated disaccharide IdoA(2*S*)-GlcNS(6S) that may play a role in high-affinity binding of BMP2. This central tri-sulfated disaccharide was common with other hexasaccharides exhibiting a high affinity for BMP2, such as dp6-P, -S, -U, -Z, and -AC. The study of dp6-K, composed of two co-eluting oligosaccharides, is very interesting. The major component of dp6-K is identical to dp6-J, but it is also composed of a minor oligosaccharide with one more sulfate, which, however, reduced the affinity compared to dp6-J only. Essentially, the central part of the minor compound is inversed compared to dp6-J with a disaccharide GlcNS (6*S*)-IdoA(2S), and the N-terminus features a GlcNAc(6S). This suggests either that the structurally inversed central part was less favorable for the binding of BMP2 or that the additional 6-O sulfate on the reducing GlcNAc was somehow destabilizing the high-affinity binding to the central part. A similar effect seemed to occur with dp6-R. In this

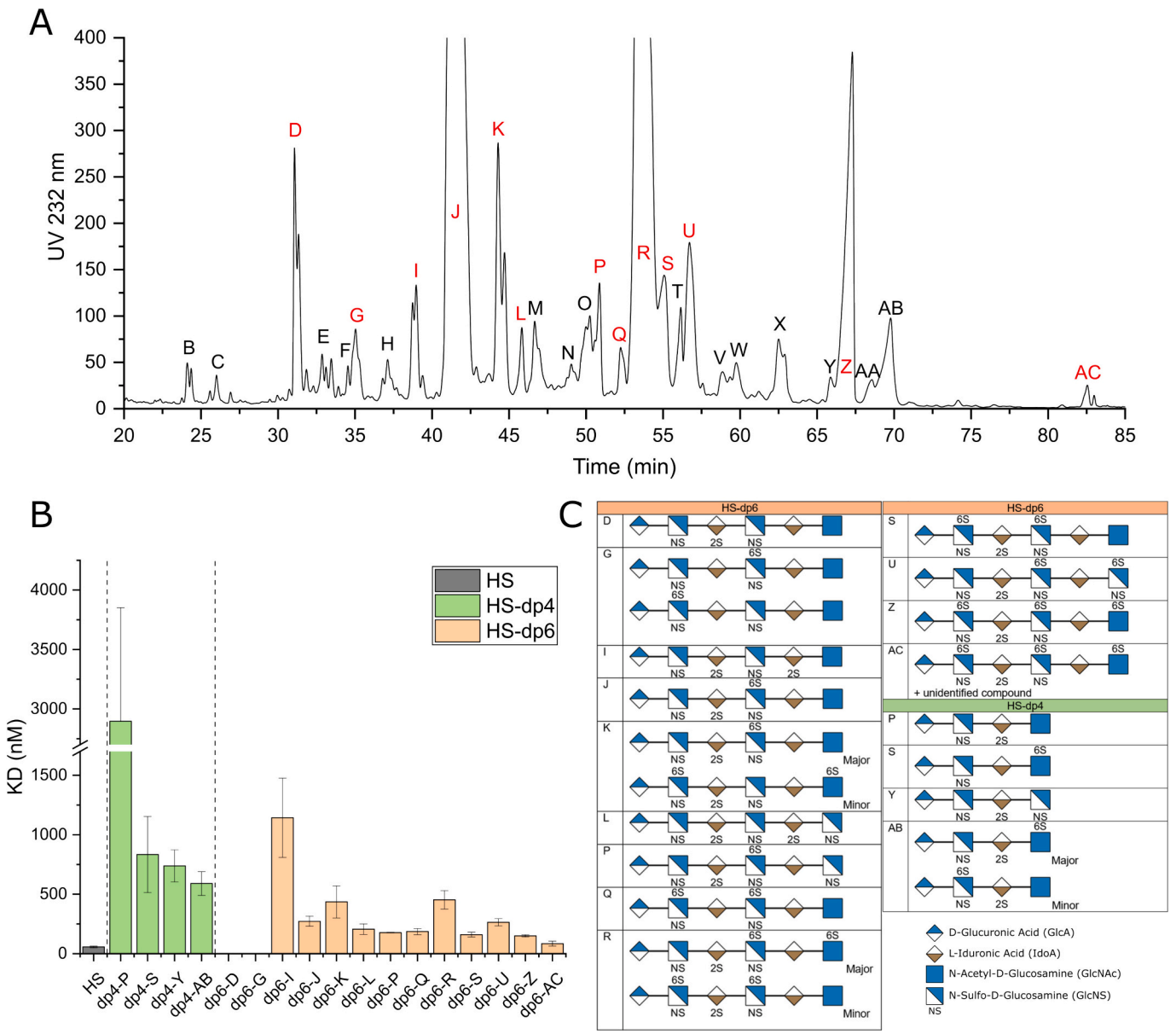

Fig. 4. Characterization of BMP2 binding on HS-oligosaccharides with defined structures.
A. SAX-HPLC separation of HS hexasaccharides. The absorbance at 232 nm detects the unsaturated bonds generated by heparinase III cleavage. The different peaks represented by letters (B to AC) were collected, and RPIP-HPLC determined their disaccharide composition. The red letters represent the oligosaccharides that were biotinylated for BLI kinetics analysis with BMP2. B. Comparison of the K_D values of BMP2 interactions with the selected oligosaccharides. For each oligosaccharide, the K_D value was measured by BLI at least in duplicate in independent experiments with a 1:1 Langmuir model on the 200 s association phase and a 40 s dissociation phase. C. Structure of selected oligosaccharides, depicted according to the Symbol Nomenclature for Glycans (SNFG, Version 1.5). Legend for symbols is represented on the bottom right. A few compounds correspond to a mixture of co-eluting species, and the major and minor components are depicted. For dp6-G, two alternative structures are possible, while there was an unidentified compound in dp6-AC (potentially 3-O sulfated).

compound, a high-affinity sequence GlcA-GlcNS(6*S*)-IdoA(2*S*)-GlcNS (6*S*)-IdoA-GlcNAc corresponding to dp6-S is present in the minority. Here again, the major component GlcA-GlcNS-IdoA(2*S*)-GlcNS(6*S*)-IdoA-GlcNAc(6S) may have decreased the overall binding affinity of dp6-R, with an isolated GlcNAc(6S) at the reducing end that could destabilize the high-affinity domain in the central region. However, this effect was not observed in the dp6-Z compound with an isolated GlcNAc (6S), which may be related to a higher sulfation in its central domain. Also, in the dp6-P, the isolated GlcNS at the reducing end seemed to have a positive effect, compared with the similar dp6-J without this additional sulfate. This would suggest that the differences in spatial positioning of the isolated N- and 6-O sulfate groups positively or negatively influence the binding of BMP2.

Altogether, our data indicate a positive role of sulfation levels and distribution, with high affinity binding achievable through locally highly sulfated motifs (such as IdoA(2*S*)-GlcNS(6S)) or a lower sulfation degree on more extended domains (dp6-L). However, these do not support the existence of a highly specific saccharide structure required for BMP2 binding, but rather that BMP2 shows a certain binding plasticity regarding interacting motifs.

3.5. *Molecular dynamic simulations of HS oligosaccharides binding to BMP2*

Computer modelling was performed to get some insights into the atomistic details of the mode of the interactions between HS fragments

and BMP2. Considering a high density of negative charge along the HS, the N-terminal ends possessing a high density of positively charged residues might be anticipated as a binding epitope of BMP2. However, the high flexibility of the N-terminal ends (Fig. Si11) makes getting the static models challenging; therefore, in the first step of modelling, the N-terminal ends were truncated. Nonetheless, molecular docking results using a truncated BMP2 revealed that even without these highly charged N-terminal ends, BMP2 offers only one epitope for HS binding (Fig. Si11). The epitope is formed at the contacts of the two subunits and located near the position of the N-terminus. During 200 ns MD simulations, the position of dp6-HS shifted slightly towards the β-strands formed by Ser12-Pro18 and Phe41-Cys47 of one of the subunits (Fig. Si12).

When the full-length BMP2 interactions with dp6-HS were simulated with aMD, the HS fragment attracted the N-terminal ends, forming a tunnel-shaped binding site (Fig. Si13A). The N-terminal ends tend to maximize the contacts with the HS fragment being stretched along the oligosaccharide so that the residues Lys3, Lys5, Arg7, Lys8, and Arg9 of both subunits could form salt bridges with the sulfate groups of the HS fragment. The contacts with the globular part of BMP2 remain comprised mainly of the residues of the loop from Ser72 to Lys76 and His44 (Fig. Si14). The interactions are stable throughout the trajectory as long as 1200 ns. The residues contacting the HS are conserved irrespective of the oligosaccharide orientation (Table Si3). Nonetheless, the binding energies depend on a balance of weak contacts varying with the exposure of sulfate groups of the HS.

When comparing the binding of two ligands to BMP2, the binding energies of the dp6-J were systematically lower than that of the dp6-I (Fig. Si15). The structure of the most favorable complex of dp6-J is characterized by the colocalization of basic residues Lys5, Arg7, Lys8, and Arg9 from both BMP2 subunits in the tight proximity of the HS' highly sulfated motif IdoA(2*S*)-GlcNS(6S) (Fig. 5).

The modelling results revealed that due to the plasticity of N-terminal ends, BMP2 may realize different modes of interactions with HS that depend on the local pattern of sulfation, namely the density of sulfation of the HS fragment and the type of sulfate group exposition. In particular, the energy-beneficial interactions with highly sulfated fragment IdoA(2*S*)-GlcNS(6S) are realized due to the increase of the local concentration of basic residues located on the flexible N-terminal ends.

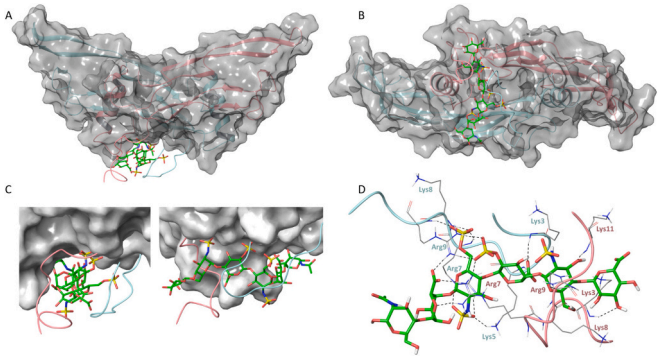

Fig. 5. The most energy-favorable complex of the full-length BMP2 dimer and dp6-J equilibrated in the course of aMD trajectory (BMP2_J_complex2.pdb): side view (A) and top view (B). Two subunits of BMP2 are shown as cartoons in pink and turquoise; the semi-transparent surface of the globular part of the protein without the N terminal ends is given in grey. The same complex zoomed on the ligand (C). The surface of the globular part of BMP2 is grey; the N-terminal tails are shown as cartoons in pink and turquoise colors to distinguish the two subunits. The basic residues of N-terminal ends of BMP2 interact with dp6-J (D). Dashed lines indicate close contacts. Ligand's C atoms are shown in green, O atoms in red, N in blue, and S in yellow.

4. Discussion

In this manuscript, we explored the molecular interactions of BMP2 with various GAGs and investigated the role of GAGs as either extracellular or cell-surface components in regulating BMP2 signaling. While csCS may enhance short-term BMP2 signaling and csHS is a regulator of BMP2 bioactivity, HS presented by the platforms (extracellular HS) is the most potent to trigger BMP2 signaling. To explore the specific HS sulfation patterns responsible for the high-affinity binding with BMP2 we generated a library of HS oligosaccharides. We demonstrated for the first time that the minimal length of HS oligosaccharides able to bind BMP2 is a tetrasaccharide (dp4), differently to what had been previously reported (Smith et al., 2018) where dp6 and 8 have been reported to be the minimal chain length required to bind BMP2. However BMP2 binds to dp4 with only moderate affinity while hexasaccharides bind with an affinity comparable to full-length HS chains. We also showed that BMP2 exhibits some structural plasticity for its binding to various HS sulfation patterns, with high affinity binding achievable through locally high sulfated domains such as (IdoA(2*S*)-GlcNS(6S)) or a lower sulfation degree on more extended domains (dp6-L).

Although the affinity of BMP2 for HS and Hep has already been explored, to our knowledge, a comparative study considering other GAGs in the same setup has never been performed. Moreover, the affinities for HS and Hep remained unclear due to important variations of K_D values reported in the literature. Indeed, the K_D of HS for BMP2 was measured at 37 nM (Billings et al., 2018) or 1.6 μM (Migliorini et al., 2017), while that of Hep ranged from 2.4 nM to 490 nM (Huegel et al., 2013; Kisiel et al., 2013; Ruppert et al., 1996). Such differences likely arise from different experimental conditions since the Hep source was identical (Sigma-Aldrich, porcine intestinal mucosa), and a SPR setup was used in all these studies. In our case, we performed several tests to identify an optimal ligand concentration for the immobilization to avoid mass transport and steric hindrance effects. We established the K_D of BMP2 interactions with HS and CS-D at 57 nM and 400 nM, respectively. However, the K_D values determined for CS-A, -E, and DS were outside the concentration range tested and should be considered cautiously. The affinities of these GAGs for BMP2 are relatively low, with a K_D in the μM range, but this does not preclude the possible physiological importance of these interactions *in vivo* (Mikami, Yasunaga, & Kitagawa, 2009). The high affinity observed for CS-D may be linked to its higher sulfation level with disulfated D-units. The CS-E, exhibiting disulfated E-units, showed a moderate affinity, possibly related to the slightly lower number of disulfated units within its chains (Supplementary Table 2) or a less affine E-unit sulfation pattern than the D unit. Although fitting the binding curves to a 1:1 binding model is not ideal, it remains the most appropriate option, given the structural heterogeneity of the GAG ligands. Furthermore, applying a more intricate model to account for this heterogeneity could introduce further bias.

When characterizing the biomimetic platforms with QCM-D, we observed different binding trends compared to BLI. The binding of BMP2 was, in this case, more critical on CS-D and CS-E, followed by HS, CS-B and CS-A. The main reason for that could be the density of GAGs, which is much lower in the BLI setup compared to QCM-D, where GAGs saturate all the binding sites of the SAv monolayer. Despite low affinity for BMP2, CS chains may sequester the protein more efficiently at high chain density.

The biomimetic platforms were used to support cellular assays to study the roles of extracellular and cell-surface GAGs in BMP2 signaling. In the literature, the role of GAGs in BMP interactions and signaling regulation has only been explored for HS and Hep, neglecting the potential roles of other GAGs such as CS and DS. We first showed that extracellular HS is more potent in inducing pSMAD1/5/9 signaling than CS, DS and HA. This result is consistent with the affinity measurement, likely due to increased BMP2 sequestered and later delivered to the cells. Supporting this idea, we also observed a small increase of pSMAD1/5/9 signaling with CS-D, although not statistically significant. Using CHO

cells, mutant for GAG synthesizing enzymes, we showed that neither, cell-surface and extracellular GAGs, are essential to generate pSMAD1/5/9 signaling, as observed with the culture HS/CS deficient cells on biomimetic platforms with cRGD only. In agreement with that, it was previously suggested that HSPGs are not essential for triggering Dosophila Dpp signaling, at least in tissues where Dpp is strongly expressed (Lin, 2004). We also showed that the EXT1 mutation in CHO pgsD-677 cells (deficient for HS) results in an increased SMAD1/5/9 phosphorylation, as observed in the literature in other cellular or mouse models (Huegel et al., 2013; Inubushi et al., n.d.). Interestingly, this increase has only been related to the lack of HS in these cells. Here, we show for the first time that this increase is associated with CS chains at the cell surface. Indeed, the signaling in HS/CS deficient cells was reduced compared to the HS mutants, returning to the same level as the wild type cells. While the role of CS in promoting signaling is evident, the influence of HS is not entirely clear. Since the number of CS chains is upregulated in KO HS (pgsD-677) compared to the wild type cells, the pSMAD1/5/9 reduction in these cells could be attributed either to an inhibitory effect of HS or to the increased availability of CS chains at the cell surface. The same trend was observed in the basal pSMAD1/5/9 levels (Fig. Si5B).

From our results, we propose that BMP2 secreted by cells in the extracellular matrix interact mainly with HS, while interactions with CS and DS are less important or null in the case of HA (Fig. 6). When getting close to the cell surface, BMP2 from the extracellular matrix or bound to GAGs can interact with either csHS, csCS or potentially directly with BMP receptors. When BMP2 binds csHS, it SMAD1/5/9 phosphorylation seems to be hindered, potentially by restraining interactions of BMP2 with its receptors. In contrast, the interactions between BMP2 and csCS promote SMAD1/5/9 phosphorylation, likely due to their transient nature that does not retain BMP2 as strongly as csHS, enabling delivery to BMP receptors (Fig. 6).

In agreement with this, Bachvarova and coworkers demonstrated that a chondroitinase treatment reduced pSMAD1/5/9 levels in chondrocytes (Bachvarova et al., 2020). Therefore, we believe that the temporal dynamics of BMP signaling induced by HS or CS chains should be the object of future studies to explore the hypotheses' validity.

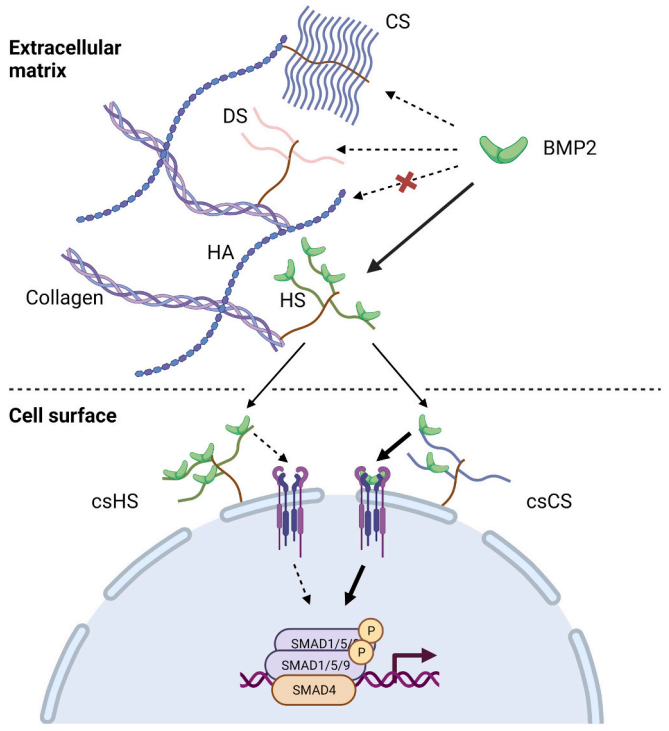

Fig. 6. Model of BMP2 interactions with extracellular and cell-surface GAGs modulating the BMP2 signaling. Image created in BioRender.com

Subsequently, we investigated whether the ability of HS to bind to BMP2 required specific sulfation patterns. To this end, a library of tetrasaccharides and hexasaccharides was generated from a natural source of HS. Hep III digestion allowed oligosaccharides to be recovered mainly from highly sulfated NS domains. Preparing defined and highly pure oligosaccharides remains a time-consuming and technical challenge (Le Pennec et al., 2023). Consequently, although the library comprised many compounds, only the few that exhibited sufficient purity levels were selected for structural and functional characterization. We first performed a disaccharide analysis to determine their disaccharide content for structural analysis of oligosaccharides. Further information about their saccharide sequence was deduced from the substrate specificity of Hep III for GlcNAc±6S-GlcA and GlcNS±6S-GlcA linkages, and disaccharide analysis of the $NaBH_4$-treated oligosaccharides, which enabled unambiguous determination of the reducing end disaccharide. We demonstrated for the first time that BMP2 could bind to HS tetrasaccharides with a moderate affinity and bound to HS hexasaccharides with an affinity close to that of intact HS chains for some of the tested species. In a previous study, Smith et al. did not detect binding of BMP2 on HS tetrasaccharides, probably related to using less sensitive, indirect SPR competition assays or less sulfated oligosaccharides. For species interacting with BMP2, although we found a positive correlation between binding and global sulfation degree, striking differences in affinity were observed for oligosaccharides exhibiting the same sulfate number, thus highlighting the importance of the sulfation pattern for the interaction. Further analysis of structure/binding relationships did not reveal an obvious specific sequence required for the interaction with BMP2, except for a central IdoA(2*S*)-GlcNS(6S) tri-sulfated disaccharide shared by several high-affinity binding oligosaccharides. It is also noteworthy that, due to the absence of commercial standards, we could not identify 3-O sulfates in our oligosaccharide library, except for the dp6-AC compound that comprised a non-identified peak. Indeed, it was previously shown that 3-O sulfated tetrasaccharides are lyase-resistant (Chopra et al., 2021; Liu & Pedersen, 2022). An oligosaccharide microarray study reported that BMP2 has some dependence on 3-O sulfate-modified HS, showing especially a high binding on hexasaccharides containing an IdoA(2*S*)-GlcNS(3S6S) (Chopra et al., 2021). Smith et al. showed that 2-O-sulfation was the least critical in BMP2 binding, compared to 6-O and the utmost important N-sulfation. Still, they had a positive effect on the BMP2 binding, stabilization, and induced SMAD1/5/9 phosphorylation. If GlcNS(3*S*6*S*)-containing compounds bind BMP2 efficiently, 3-O sulfation does not mediate the binding. Several compounds containing 3-O sulfates and other sulfates did not bind BMP2 (Chopra et al., 2021). The additional 3-O sulfate in IdoA(2*S*)-GlcNS(3S6S) moieties could contribute to increase very locally the negative charge and thus stabilize the interaction. Regarding our data, it also seems unlikely that 3-O sulfate would play a major role in BMP2 binding since the affinity of many hexasaccharides is already relatively close to that of full-length HS. BMP2 exhibits a certain plasticity for different HS sulfation types or sequences. By molecular dynamic simulations, we further demonstrate that irrespectively of the ligand orientation the binding energies of the dp6 with IdoA(2*S*)-GlcNS(6S) to BMP2 were lower than of a dp6 with four mono-sulfated monosaccharides. Few studies in the literature simulated the binding of BMP2 to HS-oligosaccharides at the atomic level. This is probably due to the complexity of the flexible N-terminal end, the conformational adjustment of which during complex formation has been considered for the first time. We proved that low-affinity HS-oligosaccharides can also be accommodated inside the flexible N-terminal end of BMP2. This plasticity could be a common feature of morphogens that require GAGs to regulate their spatial distribution and establish concentration gradients. Future studies should seek at investigating possible correlations between GAG sulfation patterns, the expression of GAG biosynthesis enzymes, and gradient of morphogens such as BMP2 *in vivo*.

CRediT authorship contribution statement

Jean Le Pennec: Writing – review & editing, Writing – original draft, Visualization, Validation, Software, Methodology, Investigation, Formal analysis, Data curation. **Olga Makshakova:** Writing – original draft, Software, Formal analysis. **Paola Nevola:** Formal analysis, Data curation. **Farah Fouladkar:** Data curation. **Evelyne Gout:** Methodology, Data curation. **Paul Machillot:** Methodology. **Mélanie Friedel-Arboleas:** Methodology. **Catherine Picart:** Writing – review & editing, Validation. **Serge Perez:** Writing – review & editing, Software, Methodology. **Andrea Vortkamp:** Writing – review & editing, Funding acquisition, Conceptualization. **Romain R. Vivès:** Writing – review & editing, Validation, Supervision, Funding acquisition, Data curation, Conceptualization. **Elisa Migliorini:** Writing – review & editing, Validation, Supervision, Resources, Project administration, Funding acquisition.

Declaration of competing interest

The authors declare that they have no known competing financial interests or personal relationships that could have appeared to influence the work reported in this paper.

Data availability

The majority of the raw data are in the supplementary information.

Acknowledgements

We acknowledge Marianne Weidenhaupt and Franz Bruckert for the useful suggestions throughout the project. This work used the platforms of the Grenoble Instruct-ERIC Centre (ISBG; UAR 3518 CNRS-CEA-UGA-EMBL) within the Grenoble Partnership for Structural Biology (PSB), supported by FRISBI (ANR-10-INBS-0005-02) and GRAL, financed within the University Grenoble Alpes graduate school (Ecoles Universitaires de Recherche) CBH-EUR-GS (ANR-17-EURE-0003). Authors acknowledge the BLI platform scientific responsible, Jean-Baptiste REISER PhD, for its help and assistance. We want to aknowledge the PTA facility, Upstream Technological Platform, for using the evaporator equipment. This work was funded by the ANR (GlyCON), grant number [ANR-19-CE13-0031-01 PRCI] and by the "Investissements d'avenir" program Glyco@Alps, grant number [ANR-15-IDEX-02]. This work has been supported by CNRS GDR 2088 "BIOMIM". IBS acknowledges integration into the IRIG (CEA).

Appendix A. Supplementary data

Supplementary data to this article can be found online at https://doi.org/10.1016/j.carbpol.2024.122294.

References

Annaval, T., Wild, R., Crétinon, Y., Sadir, R., Vivès, R. R., & Lortat-Jacob, H. (2020). Heparan sulfate proteoglycans biosynthesis and post synthesis mechanisms combine few enzymes and few core proteins to generate extensive structural and functional diversity. *Molecules, 25*(18).

Bachvarova, V., Dierker, T., Esko, J., Hoffmann, D., Kjellen, L., & Vortkamp, A. (2020). Chondrocytes respond to an altered heparan sulfate composition with distinct changes of heparan sulfate structure and increased levels of chondroitin sulfate. *Matrix Biology, 93*, 43–59.

Billings, P. C., Yang, E., Mundy, C., & Pacifici, M. (2018). Domains with highest heparan sulfate-binding affinity reside at opposite ends in BMP2/4 versus BMP5/6/7: Implications for function. *The Journal of Biological Chemistry, 293*(37), 14371–14383.

Chen, J., Sun, T., You, Y., Wu, B., Wang, X., & Wu, J. (2021). Proteoglycans and glycosaminoglycans in stem cell homeostasis and bone tissue regeneration. *Frontiers in Cell and Developmental Biology, 9*, Article 760532.

Chopra, P., Joshi, A., Wu, J., Lu, W., Yadavalli, T., Wolfert, M. A., … Boons, G.-J. (2021). The 3-O-sulfation of heparan sulfate modulates protein binding and lyase degradation. *Proceedings of the National Academy of Sciences, 118*(3).

Derynck, R., & Budi, E. H. (2019). Specificity, versatility, and control of TGF-β family signaling. *Science Signaling, 12*(570), Article eaav5183.

Diaz-Salmeron, R., Michel, J. P., Hadji, H., Gout, E., Vivès, R. R., Ponchel, G., & Bouchemal, K. (2021). Role of the interactions of soft hyaluronan nanomaterials with CD44 and supported bilayer membranes in the cellular uptake. *Colloids and Surfaces. B, Biointerfaces, 205*, Article 111916.

Djerbal, L., Vivès, R. R., Lopin-Bon, C., Richter, R. P., Kwok, J. C. F., & Lortat-Jacob, H. (2019). Semaphorin 3A binding to chondroitin sulfate E enhances the biological activity of the protein, and cross-links and rigidifies glycosaminoglycan matrices. *bioRxiv*, Article 851121.

Esko, J. D., Rostand, K. S., & Weinke, J. L. (1988). Tumor formation dependent on proteoglycan biosynthesis. *Science, 241*(4869), 1092–1096.

Esko, J. D., Stewart, T. E., & Taylor, W. H. (1985). Animal cell mutants defective in glycosaminoglycan biosynthesis. *Proceedings of the National Academy of Sciences of the United States of America, 82*(10), 3197–3201.

Essmann, U., Perera, L., Berkowitz, M. L., Darden, T., Lee, H., & Pedersen, L. G. (1995). A smooth particle mesh Ewald method. *The Journal of Chemical Physics, 103*(19), 8577–8593.

Fisher, M. C., Li, Y., Seghatoleslami, M. R., Dealy, C. N., & Kosher, R. A. (2006). Heparan sulfate proteoglycans including syndecan-3 modulate BMP activity during limb cartilage differentiation. *Matrix Biology, 25*(1), 27–39.

Hamad, O. A., Ekdahl, K. N., Nilsson, P. H., Andersson, J., Magotti, P., Lambris, J. D., & Nilsson, B. (2008). Complement activation triggered by chondroitin sulfate released by thrombin receptor-activated platelets. *Journal of Thrombosis and Haemostasis, 6*(8), 1413–1421.

Huegel, J., Mundy, C., Sgariglia, F., Nygren, P., Billings, P. C., Yamaguchi, Y., … Pacifici, M. (2013). Perichondrium phenotype and border function are regulated by Ext1 and heparan sulfate in developing long bones: A mechanism likely deranged in Hereditary Multiple Exostoses. *Developmental Biology, 377*(1), 100–112.

Inubushi, T., Nozawa, S., Matsumoto, K., Irie, F., & Yamaguchi, Y. Aberrant perichondrial BMP signaling mediates multiple osteochondromagenesis in mice. JCI Insight, 2(15), e90049.

Jones, K. B., Piombo, V., Searby, C., Kurriger, G., Yang, B., Grabellus, F., … Sheffield, V. C. (2010). A mouse model of osteochondromagenesis from clonal inactivation of Ext1 in chondrocytes. *Proceedings of the National Academy of Sciences of the United States of America, 107*(5), 2054–2059.

Jumper, J., Evans, R., Pritzel, A., Green, T., Figurnov, M., Ronneberger, O., … Hassabis, D. (2021). Highly accurate protein structure prediction with AlphaFold. *Nature, 596*(7873), 583–589.

Khodr, V., Machillot, P., Migliorini, E., Reiser, J.-B., & Picart, C. (2021). High-throughput measurements of bone morphogenetic protein/bone morphogenetic protein receptor interactions using biolayer interferometry. *Biointerphases, 16*(3), Article 031001.

Kisiel, M., Klar, A. S., Ventura, M., Buijs, J., Mafina, M.-K., Cool, S. M., & Hilborn, J. (2013). Complexation and sequestration of BMP-2 from an ECM mimetic hyaluronan gel for improved bone formation. *PLoS One, 8*(10), Article e78551.

Klüppel, M., Wight, T. N., Chan, C., Hinek, A., & Wrana, J. L. (2005). Maintenance of chondroitin sulfation balance by chondroitin-4-sulfotransferase 1 is required for chondrocyte development and growth factor signaling during cartilage morphogenesis. *Development, 132*(17), 3989–4003.

Kuo, W.-J., Digman, M. A., & Lander, A. D. (2010). Heparan sulfate acts as a bone morphogenetic protein coreceptor by facilitating ligand-induced receptor hetero-oligomerization. *Molecular Biology of the Cell, 21*(22), 4028–4041.

Laguri, C., Sadir, R., Gout, E., Vivès, R. R., & Lortat-Jacob, H. (2022). Preparation and characterization of heparan sulfate-derived oligosaccharides to investigate protein-GAG interaction and HS biosynthesis enzyme activity. *Methods in Molecular Biology, 2303*, 121–137.

Le Pennec, J., Guibert, A., Vivès, R. R., & Migliorini, E. (2024). BMP2 binds non-specifically to PEG-passivated biomaterials and induces substantial signaling. *bioRxiv* (2024.2003.2014.585026).

Le Pennec, J., Picart, C., Vivès, R. R., & Migliorini, E. (2023). Sweet but challenging: Tackling the complexity of GAGs with engineered tailor-made biomaterials. *Advanced Materials, 36*(11), Article e2312154.

Lidholt, K., Weinke, J. L., Kiser, C. S., Lugemwa, F. N., Bame, K. J., Cheifetz, S., … Esko, J. D. (1992). A single mutation affects both N-acetylglucosaminyltransferase and glucuronosyltransferase activities in a Chinese hamster ovary cell mutant defective in heparan sulfate biosynthesis. *Proceedings of the National Academy of Sciences of the United States of America, 89*(6), 2267–2271.

Lin, X. (2004). Functions of heparan sulfate proteoglycans in cell signaling during development. *Development, 131*(24), 6009–6021.

Lin, X., Wei, G., Shi, Z., Dryer, L., Esko, J. D., Wells, D. E., & Matzuk, M. M. (2000). Disruption of gastrulation and heparan sulfate biosynthesis in EXT1-deficient mice. *Developmental Biology, 224*(2), 299–311.

Liu, J., & Pedersen, L. C (2022). Emerging chemical and biochemical tools for studying 3-O-sulfated heparan sulfate. *American Journal of Physiology. Cell Physiology, 322*(6), C1166–C1175.

Matsumoto, K., Irie, F., Mackem, S., & Yamaguchi, Y. (2010). A mouse model of chondrocyte-specific somatic mutation reveals a role for Ext1 loss of heterozygosity in multiple hereditary exostoses. *Proceedings of the National Academy of Sciences of the United States of America, 107*(24), 10932–10937.

Migliorini, E., Horn, P., Haraszti, T., Wegner, S., Hiepen, C., Knaus, P., … Cavalcanti-Adam, E. (2017). Enhanced biological activity of BMP-2 bound to surface-grafted heparan sulfate. *Advanced Biosystems, 1*(4), Article 1600041.

Migliorini, E., Thakar, D., Kuhnle, J., Sadir, R., Dyer, D. P., Li, Y., … Richter, R. P. (2015). Cytokines and growth factors cross-link heparan sulfate. *Open Biology, 5*(8).

Mikami, T., Yasunaga, D., & Kitagawa, H. (2009). Contactin-1 is a functional receptor for neuroregulatory chondroitin sulfate-E *. *Journal of Biological Chemistry, 284*(7), 4494–4499.

Mottarella, S. E., Beglov, D., Beglova, N., Nugent, M. A., Kozakov, D., & Vajda, S. (2014). Docking server for the identification of heparin binding sites on proteins. *Journal of Chemical Information and Modeling, 54*(7), 2068–2078.

Mulloy, B., Gee, C., Wheeler, S. F., Wait, R., Gray, E., & Barrowcliffe, T. W. (1997). Molecular weight measurements of low molecular weight heparins by gel permeation chromatography. *Thrombosis and Haemostasis, 77*(4), 668–674.

Mundy, C., Yang, E., Takano, H., Billings, P. C., & Pacifici, M. (2018). Heparan sulfate antagonism alters bone morphogenetic protein signaling and receptor dynamics, suggesting a mechanism in hereditary multiple exostoses. *The Journal of Biological Chemistry, 293*(20), 7703–7716.

Pye, D. A., Vivès, R. R., Hyde, P., & Gallagher, J. T. (2000). Regulation of FGF-1 mitogenic activity by heparan sulfate oligosaccharides is dependent on specific structural features: Differential requirements for the modulation of FGF-1 and FGF-2. *Glycobiology, 10*(11), 1183–1192.

Pye, D. A., Vives, R. R., Turnbull, J. E., Hyde, P., & Gallagher, J. T. (1998). Heparan sulfate oligosaccharides require 6-O-sulfation for promotion of basic fibroblast growth factor mitogenic activity. *Journal of Biological Chemistry, 273*(36), 22936–22942.

Ramel, M.-C., & Hill, C. S. (2012). Spatial regulation of BMP activity. *FEBS Letters, 586*(14), 1929–1941.

Ricard-Blum, S., Vivès, R. R., Schaefer, L., Götte, M., Merline, R., Passi, A., … Nikitovic, D. (2024). A biological guide to glycosaminoglycans: Current perspectives and pending questions. *The FEBS Journal*. https://doi.org/10.1111/febs.17107. Online ahead of print.

Richard, B., Swanson, R., & Olson, S. T. (2009). The signature 3-O-sulfo group of the anticoagulant heparin sequence is critical for heparin binding to antithrombin but is not required for allosteric activation *. *Journal of Biological Chemistry, 284*(40), 27054–27064.

Ruppert, R., Hoffmann, E., & Sebald, W. (1996). Human bone morphogenetic protein 2 contains a heparin-binding site which modifies its biological activity. *European Journal of Biochemistry, 237*(1), 295–302.

Ryckaert, J.-P., Ciccotti, G., & Berendsen, H. J. C. (1977). Numerical integration of the cartesian equations of motion of a system with constraints: Molecular dynamics of n-alkanes. *Journal of Computational Physics, 23*(3), 327–341.

Sales, A., Khodr, V., Machillot, P., Chaar, L., Fourel, L., Guevara-Garcia, A., … Picart, C. (2022). Differential bioactivity of four BMP-family members as function of biomaterial stiffness. *Biomaterials, 281*, Article 121363.

Samson, S. C., Ferrer, T., Jou, C. J., Sachse, F. B., Shankaran, S. S., Shaw, R. M., … Yost, H. J. (2013). 3-OST-7 regulates BMP-dependent cardiac contraction. *PLoS Biology, 11*(12), Article e1001727.

Sefkow-Werner, J., Le Pennec, J., Machillot, P., Ndayishimiye, B., Castro-Ramirez, E., Lopes, J., … Migliorini, E. (2022). Automated fabrication of streptavidin-based self-assembled materials for high-content analysis of cellular response to growth factors. *ACS Applied Materials & Interfaces, 14*(29), 34113–34125.

Sefkow-Werner, J., Machillot, P., Sales, A., Castro-Ramirez, E., Degardin, M., Boturyn, D., … Migliorini, E. (2020). Heparan sulfate co-immobilized with cRGD ligands and BMP2 on biomimetic platforms promotes BMP2-mediated osteogenic differentiation. *Acta Biomaterialia, 114*, 90–103.

Shaffer, K. J., Smith, R. A. A., Daines, A. M., Luo, X., Lu, X., Tan, T. C., … Cool, S. M. (2024). Rational synthesis of a heparan sulfate saccharide that promotes the activity of BMP2. *Carbohydrate Polymers, 333*, Article 121979.

Siverino, C., Fahmy-Garcia, S., Niklaus, V., Kops, N., Dolcini, L., Misciagna, M. M., … Nickel, J. (2023). Addition of heparin binding sites strongly increases the bone forming capabilities of BMP9 in vivo. *Bioactive Materials, 29*, 241–250.

Smith, R. A. A., Murali, S., Rai, B., Lu, X., Lim, Z. X. H., Lee, J. J. L., … Cool, S. M. (2018). Minimum structural requirements for BMP-2-binding of heparin oligosaccharides. *Biomaterials, 184*, 41–55.

Takei, Y., Ozawa, Y., Sato, M., Watanabe, A., & Tabata, T. (2004). Three Drosophila EXT genes shape morphogen gradients through synthesis of heparan sulfate proteoglycans. *Development, 131*(1), 73–82.

Tellier, L. E., Miller, T., McDevitt, T. C., & Temenoff, J. S. (2015). Hydrolysis and sulfation pattern effects on release of bioactive bone morphogenetic protein-2 from heparin-based microparticles. *Journal of Materials Chemistry B, 3*(40), 8001–8009.

Thakar, D., Dalonneau, F., Migliorini, E., Lortat-Jacob, H., Boturyn, D., Albiges-Rizo, C., … Richter, R. P. (2017). Binding of the chemokine CXCL12alpha to its natural extracellular matrix ligand heparan sulfate enables myoblast adhesion and facilitates cell motility. *Biomaterials, 123*, 24–38.

Umulis, D., O'Connor, M. B., & Blair, S. S. (2009). The extracellular regulation of bone morphogenetic protein signaling. *Development, 136*(22), 3715–3728.

Wei, G., Bai, X., Gabb, M. M. G., Bame, K. J., Koshy, T. I., Spear, P. G., & Esko, J. D. (2000). Location of the glucuronosyltransferase domain in the heparan sulfate copolymerase EXT1 by analysis of Chinese hamster ovary cell mutants*. *Journal of Biological Chemistry, 275*(36), 27733–27740.

Wuyts, W., Van Hul, W., De Boulle, K., Hendrickx, J., Bakker, E., Vanhoenacker, F., … Willems, P. J. (1998). Mutations in the EXT1 and EXT2 genes in hereditary multiple exostoses. *American Journal of Human Genetics, 62*(2), 346–354.